This is an open access article published under a Creative Commons Attribution (CC-BY) License, which permits unrestricted use, distribution and reproduction in any medium, provided the author and source are cited.

ACS AUTHORCHOICE

THE JOURNAL OF PHYSICAL CHEMISTRY B

pubs.acs.org/JPCB Article

Effect of Aromaticity in Anion on the Cation–Anion Interactions and Ionic Mobility in Fluorine-Free Ionic Liquids

Inayat Ali Khan,* Oleg I. Gnezdilov, Yong-Lei Wang, Andrei Filippov, and Faiz Ullah Shah*

Cite This: *J. Phys. Chem. B* 2020, 124, 11962–11973

Read Online

ACCESS | Metrics & More | Article Recommendations | Supporting Information

ABSTRACT: Ionic liquids (ILs) composed of tetra(*n*-butyl)phosphonium $[P_{4444}]^+$ and tetra(*n*-butyl)ammonium $[N_{4444}]^+$ cations paired with 2-furoate $[FuA]^-$, tetrahydo-2-furoate $[HFuA]^-$, and thiophene-2-carboxylate $[TpA]^-$ anions are prepared to investigate the effects of electron delocalization in anion and the mutual interactions between cations and anions on their physical and electrochemical properties. The $[P_{4444}]^+$ cations-based ILs are found to be liquids, while the $[N_{4444}]^+$ cations-based ILs are semi-solids at room temperature. Thermogravimetric analysis revealed higher decomposition temperatures and differential scanning calorimetry analysis showed lower glass transition temperatures for phosphonium-based ILs than the ammonium-based counterparts. The ILs are arranged in the decreasing order of their ionic conductivities as $[P_{4444}][HFuA]$ (0.069 mS cm^{-1}) > $[P_{4444}][FuA]$ (0.032 mS cm^{-1}) > $[P_{4444}][TpA]$ (0.028 mS cm^{-1}) at 20 °C. The oxidative limit of the ILs followed the sequence of $[FuA]^-$> $[TpA]^-$> $[HFuA]^-$, as measured by linear sweep voltammetry. This order can be attributed to the electrons' delocalization in $[FuA]^-$ and in $[TpA]^-$ aromatic anions, which has enhanced the oxidative limit potentials and the overall electrochemical stabilities.

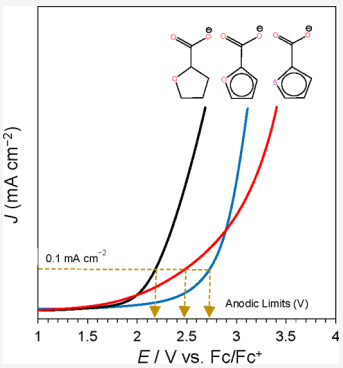

INTRODUCTION

Ionic liquids (ILs), especially room-temperature ionic liquids (RTILs), as emerging electrolytes have been extensively studied in numerous electrochemical applications owing to their exceptional physicochemical and electrochemical properties.[1−4] Some of the adoptable properties, which are common to ILs, are negligible vapor pressure, nonflammability, wide temperature range of liquid phase, high thermal stability, high solvating behavior, high ionic conductivity, and wide electrochemical stability window. ILs composed of bis(trifluoromethyl sulfonyl)imide (TFSI) anion with different nitrogen-based aromatic and aliphatic cations such as imidazolium, pyridinium, pyrrolidinium, piperidinium, and quaternary ammonium derivatives are widely used in different electrochemical applications.[5−10] The quaternary ammonium cations and their derivatives coupled with TFSI anion have good electrochemical stability at room temperature but are thermally less stable than quaternary phosphonium counterparts, and they would not be good electrolytes at high temperatures.[11,12]

There has been considerable interest in the synthesis and electrochemical characterization of phosphonium-based RTILs due to their advantages in simultaneously providing chemical, thermal, and electrochemical stabilities.[13−17] The phosphonium ILs have been used as electrolytes for various applications such as electrochemical sensing,[18] electro-polymerization of organic monomers,[19] and electrolytes in supercapacitors[20,21] and in dye-sensitized solar cells.[22,23] Many of these reported phosphonium ILs are based on large molecular weight cations derived from tris(*n*-hexyl)phosphine,[14,24] and the resulted ILs have relatively high viscosities and low ionic conductivities. Low viscosity is a main requisite for electrochemistry since viscosity pointedly affects the ionic conductivity, diffusivity, dispersion, mixing, filtration, and even equipment selections. Despite the importance of lower viscosity and higher ionic conductivity, there have been limited attempts on lowering liquid viscosities of phosphonium ILs.[25] In this regard, we have designed tetra(*n*-butyl)ammonium and tetra(*n*-butyl)-phosphonium-based ILs containing relatively smaller heterocyclic anions with a motivation to achieve the following desirable properties: (i) enhanced thermal stability (phosphonium-based ILs are known for their high chemical and thermal stabilities and comparatively low toxicity than their ammonium analogues);[11,13,26] (ii) faster diffusivity of ions (the investigation of ions self-diffusions is of great importance for ILs as electrolytes for electrochemical devices);[27,28] (iii) higher electrochemical stability (phosphonium-based ILs have wide electrochemical windows and higher ionic conductivities[13,29−31] and in some cases better electrochemical properties than their ammonium counterparts).[32]

The lowest-viscosity phosphonium-based IL for electrochemical application is tri(*n*-butyl)octylphosphonium TFSI

Received: September 15, 2020
Revised: December 2, 2020
Published: December 21, 2020

© 2020 American Chemical Society

https://dx.doi.org/10.1021/acs.jpcb.0c08421
J. Phys. Chem. B 2020, 124, 11962–11973

IL;[33] however, the viscosity is still higher in comparison to conventional TFSI-based ILs. Tsunashima and Sugiya have reported a series of ILs comprising triethylphosphine (TEP)-based cations and TFSI anions having relatively higher ionic conductivity and lower viscosity.[11] The main limitation of ILs with TFSI anions in electrochemical systems is their high fluorine content, which would lead to toxicity and environmental concerns. There have been a number of salts developed[34−37] to substitute the LIBs' electrolyte salt $LiPF_6$, but many of these salts were thermally or electrochemically unstable. In the mid-1990s, a successful attempt was made toward the synthesis of salts based on aromatic anions (following the Hückel rule) as potential battery electrolytes. This concept was strongly supported by molecular modeling.[38−40] Among the possible aromatic anions using the cyclization synthesis approach, LiTDI salt (lithium 4,5-dicyano-2-(trifluoromethyl)imidazolate) was made at a large scale.[41] Similar aromatic analogs, LiPDI (lithium 4,5-dicyano-2-(pentafluoroethyl)imidazolate) and LiHDI (lithium 4,5-dicyano-2-(*n*-heptafluoropropyl)imidazolate),[42,43] were also synthesized. The newly synthesized unique salts were thermally stable, and unlike $LiPF_6$, they were stable in the presence of moisture as well. Further, the aromatic salts (LiTDI and LiPDI) electrolytes were also highly stable on the surface of Pt electrode even in a wide potential window of 4.8 V versus Li^+/Li as confirmed by voltammetric measurements.[44] Świderski et al. studied the effect of metal cations, including Li and Na, on the electronic system of 2-furoate and thiophene-2-carboxylate.[45] Experimental and theoretical calculations showed perturbation (a disturbance of the regular elliptical motion) of the aromatic electron in the ring, which depends on the type of cations. The perturbation and polarization of the aromatic electrons in the ring further strengthened the coordination and electrostatic interaction with metal ions. In this work, the idea of aromatic anions functionalized with an electron delocalized carboxylic functional group is explored in halogen-free and highly stable ionic liquids as future potential electrolytes for electrochemical devices. The structural design of the thermally and electrochemically stable ILs is the motivation of this study, in which we focused on small phosphonium and ammonium cations and fluorine-free aromatic heterocyclic anions such as furoate $[FuA]^-$ and thiophene-2-carboxylate $[TpA]^-$ that can potentially be used as future electrolytes for electrochemical applications. Both experimental and theoretical studies have been performed in order to understand the effect of functional aromatic anions on the physical and electrochemical properties of these ILs.

EXPERIMENTAL SECTION

Chemicals and Materials. Tetra(*n*-butyl)ammonium hydroxide (Sigma-Aldrich, 40 wt % in water), tetra(*n*-butyl)phosphonium hydroxide (Sigma-Aldrich, 40 wt % in water), 2-furoic acid (Sigma-Aldrich, 98%), tetrahydro-2-furoic acid (Sigma-Aldrich, 98%), thiophene-2-carboxylic acid (Sigma-Aldrich, 98%), dichloromethane (Merck, Analytical grade), diethyl ether (Merk, Analytical grade), sodium sulfate anhydrous (VWR chemicals, 99.3%), deuterated chloroform ($CDCl_3$, Sigma-Aldrich, 99.8 at. % D, containing 0.03% (v/v) tetramethylsilane (TMS)), and ferrocene (Fc, Alfa Aesar, 99.5%) were used as received.

Synthesis of Ionic Liquids. Detailed description of the synthesis of these ILs is given in the Supporting Information (SI). In short, the ILs were synthesized by the neutralization reaction of phosphonium or ammonium hydroxide base with the corresponding cyclic carboxylic acid in a 1:1 molar ratio. After purification and drying, phosphonium-based ILs were obtained as room-temperature liquids and ammonium-based ILs were found to be semi-solids at room temperature. NMR chemical shifts, FTIR bands, and MS (ESI) data of the synthesized ionic liquids are presented in the SI.

Characterization. Bruker Ascend Aeon WB 400 (Bruker BioSpin AG, Fällanden, Switzerland) spectrometer was used for NMR analysis. The analysis medium was $CDCl_3$ with 0.03% (v/v) TMS. The working frequencies were 400.21 MHz for ^1H, 100.64 MHz for ^{13}C, and 162.01 MHz for ^{31}P. Bruker Topspin 3.5 software was used for data processing.

Fourier transform infrared (FTIR) analysis was performed on a Bruker IFS 80v vacuum FTIR machine, which is equipped with an attenuated total reflection (ATR) (liquid analysis) and with a deuterated triglycine sulfate (DTGS) detector. Forward−backward acquisition modes were used for recording spectra at room temperature. A total of 256 scans were co-added and signal-averaged at an optical resolution of 4 cm^{-1}.

Densities of the samples were measured using an Anton Paar (DMA 4100M) density meter over the range of 20−60 °C. A Lovis 2000 ME Automated Microviscometer (an Anton-Paar falling ball type viscometer with a 2.50 mm glass capillary, the viscosity range 10−10 000 cP) was used for viscosity measurements.

Thermogravimetric analysis (TGA), using a PerkinElmer 8000 TGA machine, was performed with about 2 mg of IL sample from 30 to 600 °C at 10 °C min^{-1} under nitrogen. A PerkinElmer 6000 differential scanning calorimetry (DSC) machine was used for DSC measurements. For experiments, about 3−5 mg of the IL sample was packed in an aluminum pan and heating/cooling DSC scans were recorded from −80 to 100 °C at 10 °C min^{-1}. The onset of the DSC peak was considered as the glass transition temperature (T_g). Nitrogen gas was supplied at 20 mL min^{-1} to maintain a dry environment inside the sample chamber.

Electrochemical Measurements. Metrohm Autolab (PGSTAT302N) electrochemical workstation, with FRA32 M module for impedance, was used for the electrochemical studies. About 80 μL of the electrolyte was placed in the TSC 70 closed cell. The cell was mounted onto the Microcell HC cell stand, which is connected to a temperature controller. In the Microcell HC setup, the temperature is controlled through a Peltier element which enables adjusting the temperature from −20 to 100 °C. A two-electrode cell assembly, glassy carbon electrode as working and Pt cup as counter electrodes, was used for electrochemical impedance to measure IL ionic conductivity. Impedance measurements were performed in the frequency range of 0.1 Hz to 1 MHz with an alternating current (AC) amplitude of 10 mV. Heating and cooling impedance responses were recorded from −20 to 100 °C. The cell was thermally equilibrated for at least 10 min before each measurement. The cell constant of the Pt cup was determined by means of a 100 μS cm^{-1} KCl standard solution from Metrohm (K_{cell} = 1.486 cm^{-1}). Prior to each experiment, the working electrode was polished with a Kemet diamond paste (0.25 μm). For data acquisition, Nova 2.02 software was used. In case of the ILs electrochemical stability windows (ESW) tests, linear sweep voltammetry (LSV) was run at different temperatures from −20 to 80 °C using a three-electrode cell assembly: glassy carbon (GC) as working, Ag wire (coated with AgCl) as pseudoreference, and Pt cup as counter

https://dx.doi.org/10.1021/acs.jpcb.0c08421
J. Phys. Chem. B 2020, 124, 11962−11973

electrodes, respectively. The LSV scan rate was 20 mV s^{-1}, and the applied potential was from −3 to +3 V. Ferrocene was used as an internal reference, and the potentials were converted to Fc/Fc^+ couple standard.[46] Ferrocene was poorly soluble in the IL, and an ultrasonic bath (VWR USC-TH) was employed to assist the dissolution. The current was converted to current density using the working electrode surface area (2 mm diameter). The electrochemical window of the IL was considered as the potential at 0.10 mA cm^{-2} cutoff current density.

NMR Diffusometry. Pulsed gradient spin−echo—nuclear magnetic resonance (PGSE-NMR) measurements were performed on a Bruker Avance III (Bruker BioSpin) NMR spectrometer. The working frequency for ^1H analysis was 400.27 MHz. Data were processed using Bruker Topspin 3.1 software. NMR self-diffusion measurements were performed on ^1H with a PGSE-NMR probe Diff50 (Bruker) with a maximum amplitude of the magnetic field gradient pulse of 29.73 T m^{-1}. The sample was placed in a standard 5 mm glass sample tube and closed with a plastic stopper to avoid air contact. Prior to measurements, the samples were equilibrated at a specific temperature for 30 min.

Simulation Methodology. Density functional theory (DFT) calculations were first performed to obtain optimized molecular geometries of three anions, and thereafter their tightly bound ion pair structures with tetra(*n*-butyl)ammonium and tetra(*n*-butyl)phosphonium cations, respectively, using the Gaussian 16 package (Revision B.01)[47] at the B3LYP/6-311+g(d,p) level of theory[48] with Grimme's-D3 dispersion correction.[49] Only molecular geometries with all positive vibration frequencies were taken into consideration to ensure that the obtained ion and ion pairing structures are in fact true minima in the corresponding energy landscapes.

Atomistic force field parameters for three anions based on the AMBER framework were developed in a procedure similar to that described in previous publications.[50] The CHELPG atomic partial charges for three anions were determined by fitting molecular electrostatic potentials generated from DFT calculations of individual anions at the same level of theory with B3LYP hybrid functional and 6-311+g(d,p) basis set, and thereafter uniformly down-scaled using an empirical scaling factor of 0.8 from unity ion charges to account for polarization and charge transfer effects between ion species. The cross-interaction parameters between different atom types were obtained from the Lorentz−Berthelot combination rules.

In the current work, all simulation systems are composed of 400 ion pairs having ∼26000 atoms. Atomistic molecular dynamics simulations were performed using the GROMACS package with cubic periodic boundary conditions.[51] The equations of motion were integrated using a classical velocity Verlet leapfrog integration algorithm with a time step of 1.0 fs. A cutoff distance of 1.6 nm was set for short-ranged van der Waals interactions and real-space electrostatic interactions between atomic partial charges. The particle-mesh Ewald summation method with an interpolation order of 5 and a Fourier grid spacing of 0.2 nm was employed to handle long-range electrostatic interactions in reciprocal space.

All simulation systems were first energetically minimized using a steepest descent algorithm and thereafter annealed gradually from 800 to 300 K within 20 ns. All annealed simulation systems were equilibrated in an isothermal−isobaric ensemble for 40 ns maintained using the Nosé−Hoover thermostat and the Parrinello−Rahman barostat with time coupling constants of 0.5 and 0.2 ps, respectively, to control the temperature at 300 K and the pressure at 1 atm. Atomistic simulations were further performed in a canonical ensemble for 100 ns, and simulation trajectories were recorded at an interval of 100 fs for further microstructural and dynamical analyses.

RESULTS AND DISCUSSION

The synthesized ILs, namely, tetra(*n*-butyl)phosphonium furoate ($[P_{4444}][FuA]$), tetra(*n*-butyl)phosphonium tetrahydrofuroate ($[P_{4444}][HFuA]$), tetra(*n*-butyl)phosphonium thiophenecarboxylate ($[P_{4444}][TpA]$), tetra(*n*-butyl)ammonium furoate ($[N_{4444}][FuA]$), tetra(*n*-butyl)ammonium tetrahydrofuroate ($[N_{4444}][HFuA]$), and tetra(*n*-butyl)ammonium thiophenecarboxylate ($[N_{4444}][TpA]$), are obtained in good yields. The structures and abbreviations of the ions in these ILs are shown in Figure 1.

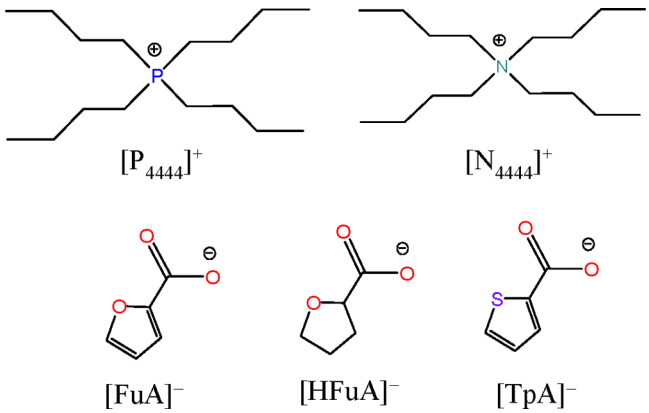

Figure 1. Chemical structures and abbreviations of the ionic components of the synthesized ILs.

The synthesized ILs were characterized by ^1H, ^{13}C, and ^{31}P NMR analyses to confirm the structures and purity of the products. The ^1H NMR spectra (SI Figure S1, Figure S4, and Figure S7) of $[P_{4444}][FuA]$, $[P_{4444}][TpA]$, and $[P_{4444}][HFuA]$ have three resonance lines associated with the alkyl chains of the phosphonium cation; a triplet in the range from 0.90 to 0.95 ppm is for the terminal methyl groups, a multiplet between 1.46 and 1.54 ppm is for all of the methylene protons, and another multiplet between 2.30 and 2.46 ppm is due to the 8 α-protons. The downfield resonance lines of varying multiplicity in the ranges of 6.32−6.34 ppm (multiplet) and 6.88−6.90 ppm (multiplet) and at 7.34 ppm (singlet) are assigned to the three non-equivalent protons of the furoate anion (Figure S1). Similar varying multiplicities were also observed for the three non-equivalent protons of thiophenecarboxylate anion at 6.97−6.99 pm (triplet), 7.32−7.33 pm (doublet), and 7.66−7.67 ppm (doublet), as shown in Figure S4. The protons in tetrahydrofuroate ring have a different pattern of resonance lines because of the saturated structure and chiral conformation. The resonance multiplicity at 4.38−4.42 ppm is assigned to the single proton attached to the carbon at position 2. The second more deshielded protons attached to carbon at position 5 have multiple resonance lines from 3.79 to 4.01 ppm. The third deshielded protons attached to carbon at position 3 have two separate multiplicities, one from 2.19 to 2.26 ppm and another from 1.97 to 2.02 ppm. Protons attached to carbon at position 4 have a resonance line (multiple) at 1.85−1.92 ppm, Figure S7. In the ^1H NMR

https://dx.doi.org/10.1021/acs.jpcb.0c08421
J. Phys. Chem. B 2020, 124, 11962−11973

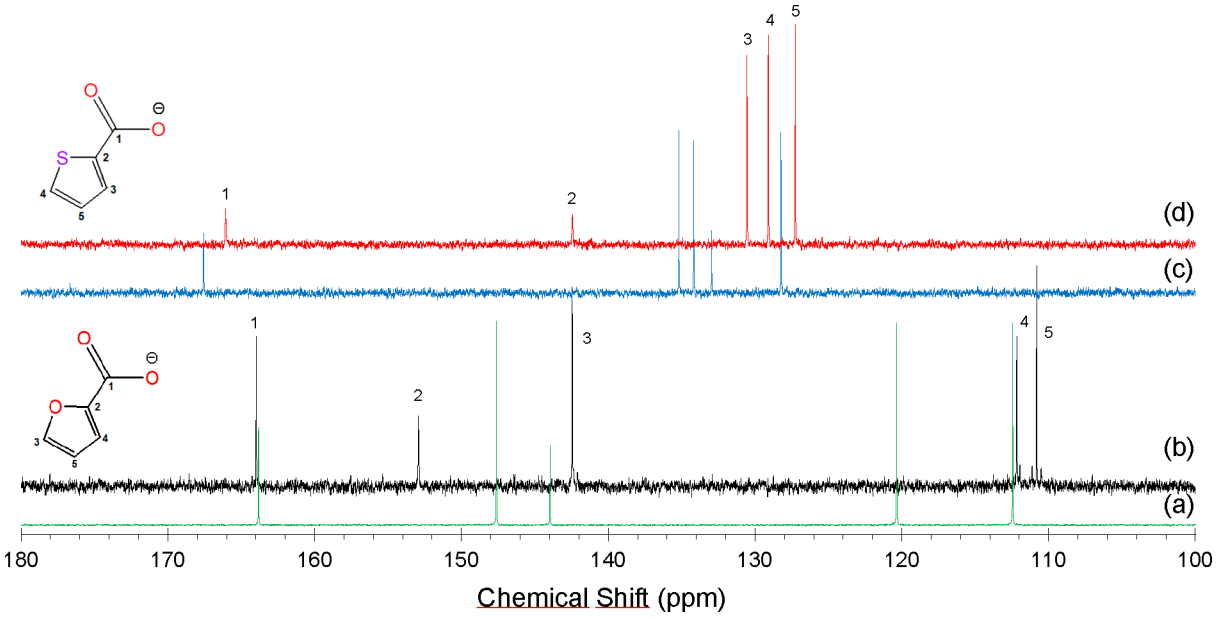

Figure 2. ^{13}C NMR spectra in the range from 100 to 180 ppm: (a) 2-furoic acid, (b) [P_{4444}][FuA] showing peaks of furoate anion, (c) thiophene-2-carboxylic acid, and (d) [P_{4444}][TpA] showing peaks of thiophene-2-carboxylate anion.

spectra, the absence of a resonance line corresponds to -OH of 2-furoic acid, tetrahydro-2-furoic acid, and thiophene-2-carboxylic acid in the range of 8.54−10.00 ppm, confirming the successful synthesis and purity of the respective ILs.

The ^{13}C NMR spectra of the ILs (Figure S2, Figure S5, and Figure S8) have upfield resonance lines from 13.61 to 24.21 ppm associated with the aliphatic carbon chains of the phosphonium cation. For [P_{4444}][FuA] (Figure S2), the downfield resonance lines at 110.8, 112.2, 142.4, and 152.93 ppm are accounted for by the four carbon atoms in the furoate ring, while the resonance line at 163.9 ppm is attributed to the carboxylate carbon. In case of [P_{4444}][TpA] (Figure S5), the resonance lines at 127.2, 129.1, 130.5, and 142.4 ppm are assigned to the carbons in the thiophenecarboxylate ring, while the resonance line at 166.1 ppm is for the carboxylate carbon. For [P_{4444}][HFuA] (Figure S8), the ^{13}C resonance lines at 25.5, 30.6, 69.1, and 77.8 ppm are attributed to the carbons in the tetrahydrofuroate ring, while the resonance line at 176.5 ppm is due to the carboxylate carbon. In the ^{13}C NMR spectra of [P_{4444}][FuA], the signals from C3, C4, and C5 carbons (in furoate anion) are shifted upfield while the signals from C1 and C2 carbons (in furoate anion) are shifted downfield in comparison with the chemical shifts present in the spectra of 2-furoic acid, Figure 2a,b. It means an increase in electronic charge density around C3, C4, and C5 carbon atoms and decrease around C1 and C2 carbon atoms in the ILs compared with free acid.[45] This is due to the electron aromaticity and delocalization from the carbonyl group toward the furan ring. In the spectra of [P_{4444}][TpA], signals arising from C1, C3, C4, and C5 carbons (in thiophene-2-carboxylate anion) are shifted upfield while the signal from the C2 carbon (in thiophene-2-carboxylate anion) is shifted downfield in comparison with the chemical shifts present in the spectra of thiophene-2-carboxylic acid, Figure 2c,d. It means higher electronic densities on C1, C3, C4, and C5 carbon atoms and lower electronic density on C2 carbon atom.[45] The C2 carbon in thiophene-2-carboxylate anion is more deshielded due to the ring aromaticity along with electron-withdrawing effect of the carbonyl group. The difference in chemical shifts of C1 carbon signals (Figure 2b,d) is due to the presence of oxygen in furoate anion ring and sulfur in thiophene-2-carboxylate anion ring. The ^{31}P NMR spectra (Figure S3, Figure S6, and Figure S9) exhibit a single resonance line at 33.05 ppm in the case of [P_{4444}][FuA] and at 33.02 ppm in the case of both [P_{4444}][TpA] and [P_{4444}]-[HFuA] associated with the phosphorus atom present in the phosphonium cation. The synthesized ILs are also characterized by electrospray ionization mass spectrometry (ESI-MS) to further confirm synthesis and purity. The ESI-MS mass to charge ratio values and spectra are given in the Supporting Information (Figures S10−S15). The mass to charge ratios detected are assigned to phosphonium (m/z 259.25), ammonium (m/z 242.28) cations and fuorate (m/z 111.01), thiophene-2-carboxylate (m/z 126.99), and tetrahydrofuorate (m/z 115.04) anions. The mass to charge ratio values are very much close to the calculated values.

The ATR-FTIR spectra of the ILs (Figure S16) have stretching bands at 2957−2870 cm^{-1} due to the sp^2 and sp^3 C−H functional groups. The vibrational bands in the range of 650 to 570 cm^{-1} can be assign to the P−C stretching in the phosphonium cation.[52] A strong band at 1100−1083 cm^{-1} is assigned to the stretching of the C−O functional group. The FTIR band of C═O stretching generally appears at about 1700 cm^{-1}. However, the exact position of this band is dependent on the nature of the functional groups such as carboxylic acid, ester, aldehyde, and ketone and the chemical environment of C═O such as aromatic delocalization of electrons and electron-withdrawing effect. Figure 3 shows the FTIR spectra of ILs in the region of 1850 to 1150 cm^{-1}. The infrared bands observed at 1750−1720 cm^{-1} (with shoulders at 1666 cm^{-1}) in the spectra of [N_{4444}][FuA], [N_{4444}][HFuA], [N_{4444}][TpA], and [P_{4444}][HFuA] are assigned to the carbonyl stretching of [HFuA]$^-$ and [FuA]$^-$ anions. The carbonyl stretching is shifted to lower wavenumber of 1704 cm^{-1} in [FuA]$^-$ anion and of 1680 cm^{-1} in [TpA]$^-$ anion in [P_{4444}][FuA] and [P_{4444}][TpA] ILs.

https://dx.doi.org/10.1021/acs.jpcb.0c08421
J. Phys. Chem. B 2020, 124, 11962−11973

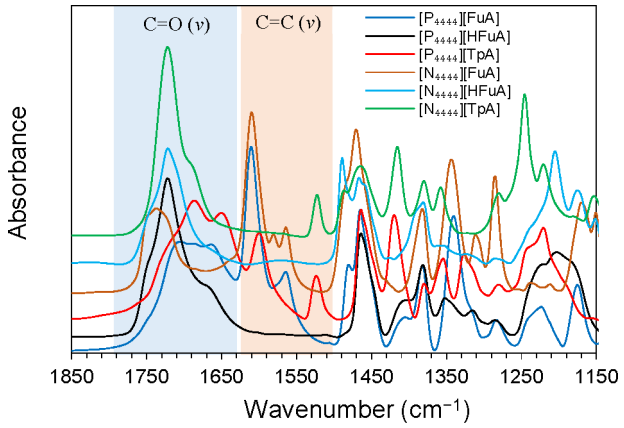

Figure 3. ATR-FTIR spectra of the ILs in the frequency range from 1850 to 1150 cm^{-1}.

The shifting in carbonyl stretching frequencies to lower values is due to a more single-bond character, which arises due to the electron delocalization of the carbonyl double bond toward the rings in $[FuA]^-$ and $[TpA]^-$ anions. This electron delocalization favors the overall stability of $[P_{4444}][FuA]$ and $[P_{4444}][TpA]$ ILs. The shift in carbonyl stretching frequencies toward lower values is not very prominent in the case of $[N_{4444}][FuA]$ and $[N_{4444}][TpA]$ ILs, which is probably due to the more electronegative nitrogen atom that can polarize the electron density more toward the cation, and restrict the electron circulation over the conjugated ring. Similarly in phosphonium-based ILs, the vibrational frequencies associated with the C═C stretching are also shifted to lower values of 1610−1566 cm^{-1} for $[FuA]^-$ and 1602−1525 cm^{-1} for $[TpA]^-$ in comparison to the reference values of 1650−1566 cm^{-1} for the cyclic alkenes. The bending vibrational frequencies at 1477−1420, 1385−1342, and 920 cm^{-1} are attributed to ═C−H, -C−H, and C═C functional groups, respectively. An IR band characteristic of OH (3400−3100 cm^{-1}; expected for the -OH group in the cyclic carboxylic acids) has not been observed, confirming the successful formation of anion. The electron delocalization is further confirmed by DFT calculations. It is shown that the optimized anion structure of $[HFuA]^-$ is characterized by tilted nonplanar configuration with localized charge density distribution (Figure 4a). However, both $[FuA]^-$ and $[TpA]^-$ are characterized by planar structures due to the formation of a conjugated structure between the heteroaromatic rings and the carboxylate moieties. The charge density distribution on $[FuA]^-$ anion framework (Figure 4b) is mainly concentrated around the oxygen unit on heteroaromatic ring moiety and the carboxylate moiety. This indicates that the charge density distribution in $[FuA]^-$ is more delocalized than that on $[HFuA]^-$ anion. The replacement of oxygen atom on heteroaromatic ring moiety with sulfur atom can further strengthen the charge delocalization around the whole anion framework (Figure 4c).

The charge delocalization effects on these three anions are further manifested on the HOMO (highest occupied molecular orbital) and LUMO (lowest unoccupied molecular orbital) energies. Figure 5 presents the molecular orbital energies from HOMO−5 to LUMO+5, the HOMO−LUMO energy gap, and the charge density contours of three anions at HOMO and LUMO states. The charge delocalization effect for three anions are characterized by $[HFuA]^-$ < $[FuA]^-$ < $[TpA]^-$, and therefore the HOMO energies are gradually lowered from $[HFuA]^-$ to $[TpA]^-$ with a concomitant increase in LUMO energies and the enlarged energy gaps (E_{LUMO}−E_{HOMO}), indicating that the former is relatively easier and the latter is harder to oxidize. This is further confirmed by the thermo-electrochemical stabilities (the LSV curves shown in Figure 10) of ILs consisting of these anions coupled with $[P_{4444}]^+$ cations. The variations of HOMO and LUMO energies are detailed in the corresponding electron density contours shown in Figure 6. The NMR, FTIR, and the DFT calculations confirmed the electrons' delocalizations in $[FuA]^-$ and $[TpA]^-$ anions over the aromatic rings that might have a pronounced impact on the physiochemical and electrochemical properties of the synthesized ILs.

The properties of ILs such as thermal behavior and stability, viscosities, ionic conductivity, diffusivity, and electrochemistry are significantly affected by impurities of IL samples.[50,53,54] Among all possible impurities, water holds a peculiar significance.[50,53,54] Therefore, the water content in IL samples was determined, and it was found to be within the acceptable limits such as 300 ppm in $[P_{4444}][FuA]$, 280 ppm in $[P_{4444}][HFuA]$, and 360 ppm in $[P_{4444}][TpA]$. The ammonium-based ILs are semi-solids at room temperature; therefore, their viscosities and ionic conductivities are not measured. However, the phosphonium-based ILs are viscous liquids at room temperature and their densities and viscosities in the temperature range from 20 to 60 °C are presented in Table S1. In addition, the liquid density data for tetra(*n*-butyl)phosphonium-based ILs obtained from atomistic simulations are consistent with experimental results. As expected, the densities of these ILs are linearly decreased with increasing temperature. The comparatively high density of $[P_{4444}][TpA]$ at all temperatures is consistent with the presence of high atomic mass sulfur atom in $[TpA]^-$ anion. As shown in Table S1, viscosity decreases with temperature; i.e., the viscosity of $[P_{4444}][FuA]$ is 955.6 mPa s at 25 °C, which is decreased to 98.32 mPa s at 60 °C. Chemical structures, electrostatic

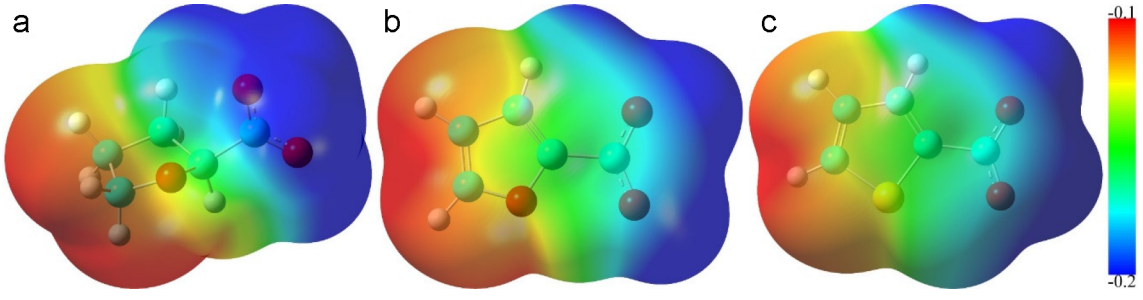

Figure 4. Molecular electrostatic potential contours of (a) $[HFuA]^-$, (b) $[FuA]^-$, and (c) $[TpA]^-$ anions obtained from DFT calculations.

https://dx.doi.org/10.1021/acs.jpcb.0c08421
J. Phys. Chem. B 2020, 124, 11962−11973

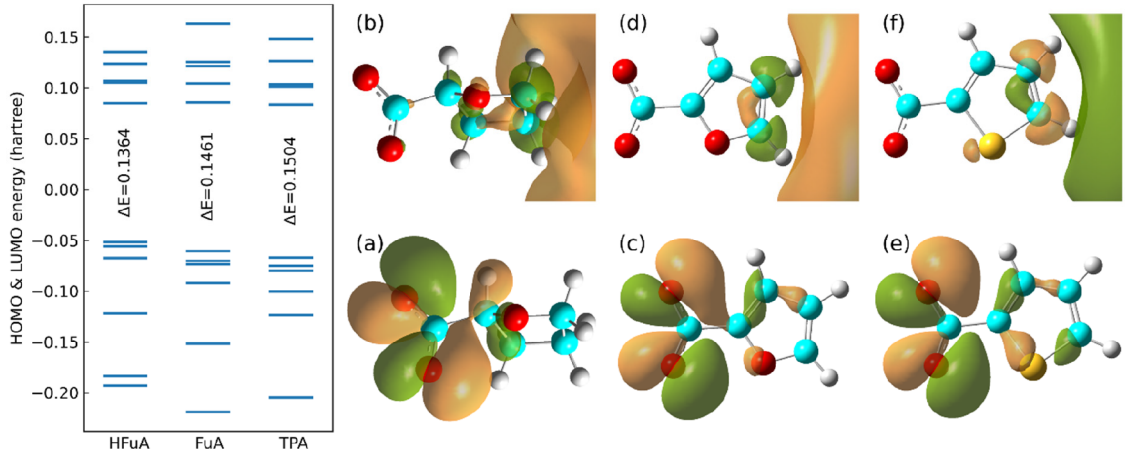

Figure 5. Molecular orbital energies from HOMO−5 to LUMO+5, the HOMO−LUMO energy gap, and the electron density contours of anions at HOMO and LUMO states: (a, c, and e) HOMOs for $[HFuA]^-$, $[FuA]^-$, and $[TpA]^-$ anions, and (b, d, and f) LUMOs for these three anions.

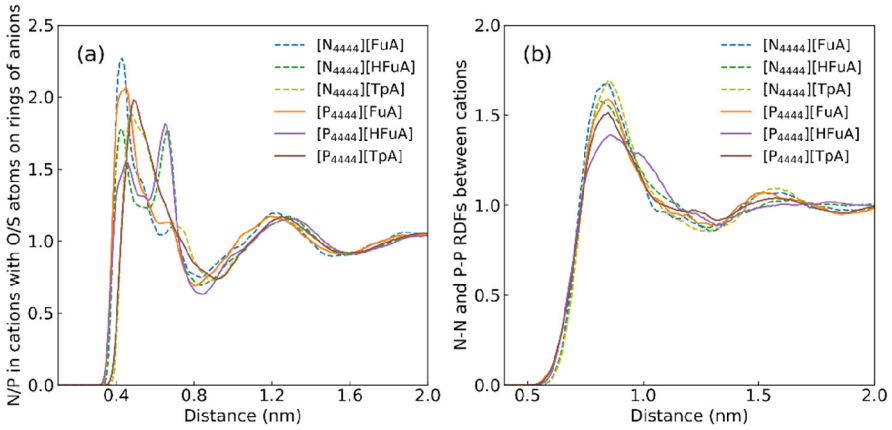

Figure 6. Intermolecular RDFs of (a) N/P in cations with O/S atoms on aromatic rings of anions and (b) N−N and P−P pairs between cations.

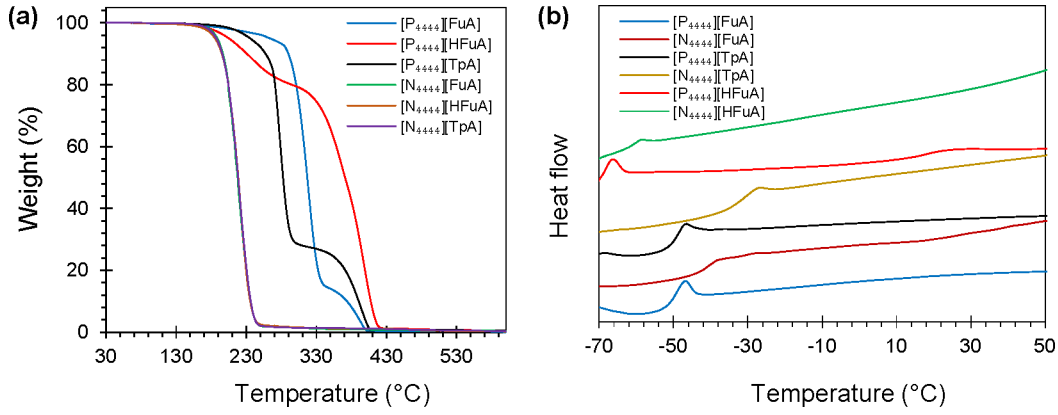

Figure 7. TGA thermograms (a) and DSC scan curves (b) of the ILs.

interactions among ionic species, hydrogen bonding, and alkyl-chain stacking interactions are the main factors affecting the physical state and viscosity of these synthesized ILs. The radial distribution functions (RDFs) for the cation−anion and cation−cation pairs are presented in Figure 6a,b. The cations' central atoms N and P while the anions' central atoms O or S were taken as reference to calculate the site−site RDFs that would present the microscopic structure between ionic species. In the RDFs presented in Figure 6a, two distinct solvation shells are observed at around 0.5 and 1.3 nm for the $[N_{4444}]^+$ and $[P_{4444}]^+$ cations with $[FuA]^-$, $[HFuA]^-$ and $[TpA]^-$ anions. Comparatively broader distribution is observed for [HFuA]-based ILs. A higher first peak and lower first minimum have been observed in the cation−anion RDFs for the same anion with alkylammonium and alkylphosphounium cations, showing a well-define solvation shell of the anions around cations and vice versa. This means that the aromatic anions such as $[FuA]^-$ and $[TpA]^-$ have stronger intermolecular interactions with the tetra(*n*-butyl)ammonium and tetra(*n*-butyl)phosphonium cations than the nonaromatic

https://dx.doi.org/10.1021/acs.jpcb.0c08421
J. Phys. Chem. B 2020, 124, 11962−11973

$[HFuA]^-$ anion. Similar cation−anion RDFs calculations have been reported for the alkylphosphonium orthoborate ILs.[50] The cation−cation RDFs (Figure 6b) exhibit a broad first maxima with some distance shoulder which is presenting an ionic system dominated by a long-range electrostatic interaction.[50] This is specially observed for tetra(*n*-butyl)-ammonium cations having stronger interactions with neighboring cations than their phosphonium counterparts (Figure 6b) when they are coordinated with the same anion. This supports the semi-solid nature of the tetra(*n*-butyl)ammonium ILs at room temperature. The RDFs calculations clearly show that the local ionic structures of the ILs are affected by the nature of the cations and anions.

Thermal properties of the ILs are determined using TGA and DSC. The most significant descriptor in TGA analysis is the decomposition onset temperature (T_d), which is the intersection of the baseline and the tangent of the weight versus temperature (Figure S17). The T_d depends on the intrinsic stability and mutual interactions between ions.[55] The TGA curves of the ILs shown in Figure 7a indicate that these ILs have two inflection points, corresponding to two decomposition steps. The majority of the weight loss for $[P_{4444}][FuA]$ (79%) and $[P_{4444}][TpA]$ (71%) comes from the first inflection, while most of the weight loss for $[P_{4444}][HFuA]$ (70%) comes from the second inflection that corresponds to the cation decomposition. The T_d (onset temperatures from the first inflection point) of $[P_{4444}][FuA]$, $[P_{4444}][HFuA]$, and $[P_{4444}][TpA]$ are 291, 208, and 262 °C, respectively (Table 1).

Table 1. Molecular Weights, Glass Transition Temperatures, Decomposition Temperatures, and Ionic Conductivity of the Synthesized ILs

IL	MW (g mol^{-1})	T_g (°C)	T_d (°C)	σ (mS cm^{-1}) at 20 °C
$[P_{4444}][FuA]$	370.5	−55.62	291	0.032
$[P_{4444}][HFuA]$	374.5	−68.21	208	0.069
$[P_{4444}][TpA]$	386.6	−55.65	262	0.028
$[N_{4444}][FuA]$	353.5	−45.41	197	
$[N_{4444}][HFuA]$	357.6	−66.25	201	
$[N_{4444}][TpA]$	369.6	−37.43	197	

Conversely, the ammonium-based ILs exhibit single-step decomposition TGA curves (Figure 7a) with T_d at about 200 °C. Ohno and co-workers have reported a series of tetra(*n*-butyl)phosphonium-based amino acid ILs having higher thermal stabilities than imidazolium- and ammonium-based ILs.[26] $[P_{4444}]$[succinate] and $[P_{4444}]$[maleate] are liquids, while $[P_{4444}]$[fumarate] is solid at room temperature.[56] The T_d temperatures reported for the phosphonium-based ILs were 276, 264, and 265 °C with succinate, maleate, and fumarate anions,[56] while, with choline-based ILs, have the T_d temperatures of 212, 223, and 219 °C with succinate, maleate, and fumarate anions,[57] respectively. On the other hand, choline-based ILs with a range of amino acids anions are known to decompose at temperatures < 200 °C.[58] The effect of cations on the thermal decomposition of furoate-based ILs have also been reported.[59] A decrease in thermal stability was observed by changing the cation from phosphonium to ammonium; i.e., the $[P_{4442}][FA]$ IL has T_d of 289 °C, while $[N_{4442}][FA]$ IL has T_d of 198 °C.[59] The DSC heating scans at a rate of 10 °C min^{-1} are shown in Figure 7b, where we can see that each IL exhibits a heat capacity change that corresponds to a glass transition temperature (T_g). In comparison to the phosphonium counterparts, the T_g values are positively shifted with ammonium cations, Figure 7b and Table 1. The subzero T_g values of the ILs indicate the very low crystallization rate and fairly stable supercooling state. The thermal analysis shows that the synthesized ILs have relatively high thermal stability and lower glass transition temperatures. The high thermal stability and subzero glass transition temperatures of these ILs make them excellent electrolytes for electrochemical devices operating at variable temperatures.

Figure 8 shows temperature-dependent ionic conductivities of the phosphonium-based ILs. The original ionic conductivity

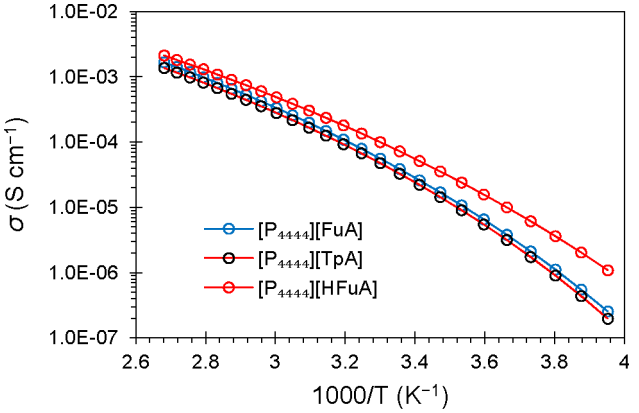

Figure 8. Temperature-dependent ionic conductivity of the phosphonium-based ILs.

data as a function of temperature are provided in Figure S18 in the SI. At 20 °C, the ionic conductivities of ILs with a common cation can be arranged in decreasing order as $[P_{4444}][HFuA]$ (0.069 mS cm^{-1}) > $[P_{4444}][FuA]$ (0.032 mS cm^{-1}) > $[P_{4444}][TpA]$ (0.028 mS cm^{-1}) (Table 1). The ionic conductivities of $[P_{4444}][FuA]$ and $[P_{4444}][TpA]$ are lower than $[P_{4444}][HFuA]$ over the whole temperature range. The ionic conductivity of $[P_{4444}][TpA]$ is slightly lower than $[P_{4444}][FuA]$. The difference in ionic conductivities of these ILs for the same cation is attributed to the variations in microstructures of the three anions and their varied charge delocalization effect, which in turn affect their ionic mobility.

The Vogel−Fulcher−Tamman (VFT) equation (eq 1) was used to fit the temperature (K) versus ionic conductivity plots of the phosphonium-based ILs in the temperature range from −20 °C (253 K) to 100 °C (373 K).

$$\sigma = \sigma_o \exp \frac{(-B)}{(T - T_o)} \quad (1)$$

where σ_o (S cm^{-1}), B (K), and T_o (K) are the fitting parameters. σ_o is a pre-exponential factor, B is a factor related to the activation energy (E), and T_o is the ideal glass transition temperature, respectively. The plots of temperature versus ionic conductivities for $[P_{4444}][HFuA]$, $[P_{4444}][FuA]$, and $[P_{4444}][TpA]$ are well-fitted to the VFT model over the whole temperature range, Figure 8. The best-fit parameters of eq 1 are given in Table 2. T_o is found to be about 60 K below the experimental T_g values, which is typical for ionic liquids.[60] There is a direct relation between B and activation energy for ion conduction ($E_\sigma = BR$). As can be seen in Table 2, the E_σ value is increasing from 12.1 kJ mol^{-1} for $[P_{4444}][TpA]$ to 13.6 kJ mol^{-1} for $[P_{4444}][HFuA]$ due to the slower mobility of ions

https://dx.doi.org/10.1021/acs.jpcb.0c08421
J. Phys. Chem. B 2020, 124, 11962−11973

Table 2. VFT Equation Parameters for the Ionic Conductivity Data of the Phosphonium-Based ILs

IL	σ_o (S cm^{-1})	B (K)	T_o (K)	E_σ (kJ mol^{-1})
[P_{4444}][FuA]	2.2 ± 0.05	1565 ± 6.7	155 ± 1	13.0 ± 0.05
[P_{4444}][TpA]	1.3 ± 0.07	1460 ± 14	160 ± 1	12.1 ± 0.12
[P_{4444}][HFuA]	2.5 ± 0.20	1640 ± 25	141 ± 1	13.6 ± 0.20

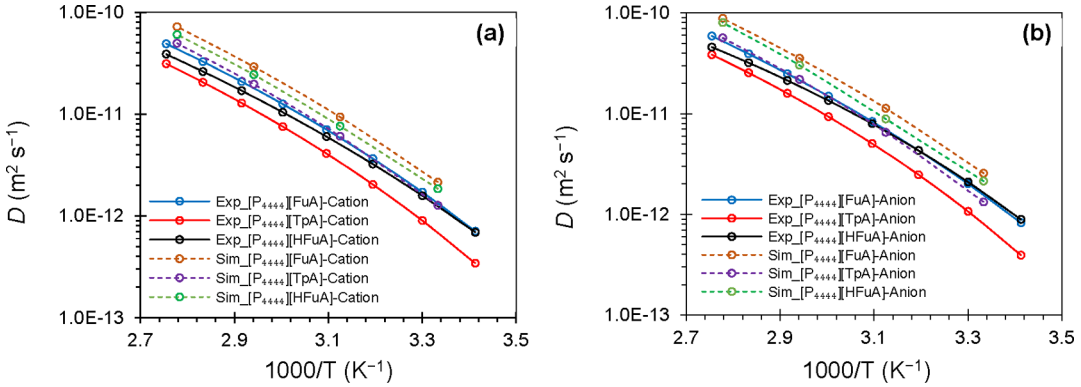

Figure 9. Temperature-dependent self-diffusion coefficients of the cations (a) and anions (b) in tetra(*n*-butyl)phosphonium-based ILs.

as a result of heterogeneous interactions among neighboring ions and the specific microstructures in the IL matrices.

The self-diffusion coefficients of ions in the phosphonium-based ILs is evaluated using PGSE-NMR technique. The self-diffusion coefficients of cations and anions in each IL can be separately determined since these ILs have NMR active proton (^{1}H) nuclei in their respective ion groups. In addition, the self-diffusion coefficients of [P_{4444}]$^+$ cation and their coupled three anions are also calculated from atomistic simulations. Tables S2 and S3 show that the experimental and computational self-diffusion coefficients have similar trends of ions diffusivity in the [P_{4444}][FuA], [P_{4444}][HFuA], and [P_{4444}][TpA] ILs with increasing temperature.

The experimental and computational self-diffusion coefficients of the anions and cations in [P_{4444}][FuA], [P_{4444}]-[HFuA], and [P_{4444}][TpA] ILs versus temperature are fitted to VFT equation for diffusivity (eq 2), and the data are shown in Figure 9.

$$D = D_o \exp \frac{(-B)}{(T - T_o)} \quad (2)$$

where D_o (m^2 s^{-1}), T_o (K), and B (K) are adjustable parameters. Energy of activation for diffusion is related to B ($E_D = BR$). The values of the best-fit parameters are tabulated in Table 3. The solid and dashed lines in Figure 9 are the calculated curves using eq 2. It is worth mentioning that the experimental and simulated diffusion coefficients for the anions in each IL are larger than those for the corresponding cations. This is due to the smaller sizes of these anions as compared with the [P_{4444}]$^+$ cation. The diffusivities of the cation and anions in [P_{4444}][FuA] and [P_{4444}][HFuA] are comparable with and higher than [P_{4444}][TpA]. This is due to the enhanced intermolecular interactions of [TpA]$^-$ anions with neighboring ionic species than those in the other two ILs. The experimental values of T_o and E_D are slightly larger than the simulated values. This can be attributed to the fact that the simulation measurements may not include all of the smaller interactive forces which exist between the ions in experimental measurements. In the case of [P_{4444}][HFuA], the simulated T_o value for the cation (145 K) is larger than that for the anion (115 K), which means that the [HFuA]$^-$ anions are clustered and have adopted a glassy physical state at earlier temperature than the [P_{4444}]$^+$ cation (Table 3).

Table 3. VFT Equation Parameters of Self-Diffusion Coefficient of the Cations and Anions in Tetra(*n*-butyl)phosphonium-Based ILs

Experimental				
ion	$D_o \times 10^{-8}$ (m^2 s^{-1})	B (K)	T_o (K)	E_D (kJ mol^{-1})
[P_{4444}]$^+$	7.50 ± 0.18	1400 ± 8.3	172 ± 1	11.6 ± 0.07
[FuA]$^-$	9.50 ± 0.38	1410 ± 13	172 ± 2	11.7 ± 0.11
[P_{4444}]$^+$	4.00 ± 0.25	1295 ± 15	182 ± 2	10.8 ± 0.13
[TpA]$^-$	5.60 ± 0.46	1320 ± 21	182 ± 2	11.0 ± 0.17
[P_{4444}]$^+$	5.80 ± 0.29	1440 ± 14	166 ± 2	12.0 ± 0.12
[HFuA]$^-$	6.30 ± 0.54	1420 ± 26	166 ± 2	11.8 ± 0.21
Simulated				
ion	$D_o \times 10^{-7}$ (m^2 s^{-1})	B (K)	T_o (K)	E_D (kJ mol^{-1})
[P_{4444}]$^+$	2.20 ± 0.09	1580 ± 10	163 ± 1	13.1 ± 0.1
[FuA]$^-$	2.70 ± 0.11	1580 ± 11	163 ± 1	13.1 ± 0.1
[P_{4444}]$^+$	1.08 ± 0.08	1420 ± 09	175 ± 1	11.8 ± 0.2
[TpA]$^-$	1.55 ± 0.11	1470 ± 12	174 ± 2	12.2 ± 0.1
[P_{4444}]$^+$	5.30 ± 0.10	1950 ± 11	145 ± 2	16.2 ± 0.1
[HFuA]$^-$	5.50 ± 0.12	2730 ± 14	115 ± 1	22.7 ± 0.2

The ESW of an IL is the potential range in which it does not get oxidized or reduced, which can be calculated by subtracting the reduction potential limit (cathodic limit, E_C) from the oxidation potential limit (anodic limit, E_A). In order to make a base for the ESW determination, a current density called cutoff current density must be selected to evaluate the redox potentials. Water content and the operating temperatures are among the main factors affecting the ESW of an IL. Generally, increasing temperature and water content results in narrowing of both E_C and E_A and subsequently reducing the ESW of ILs.[54,61]

The LSV characterization at variable temperatures is carried out to evaluate the thermo-electrochemical stabilities of the synthesized ILs. The LSV curves of the phosphonium-based ILs at 20 °C are shown in Figure 10a. Both the [P_{4444}][FuA]

https://dx.doi.org/10.1021/acs.jpcb.0c08421
J. Phys. Chem. B 2020, 124, 11962−11973

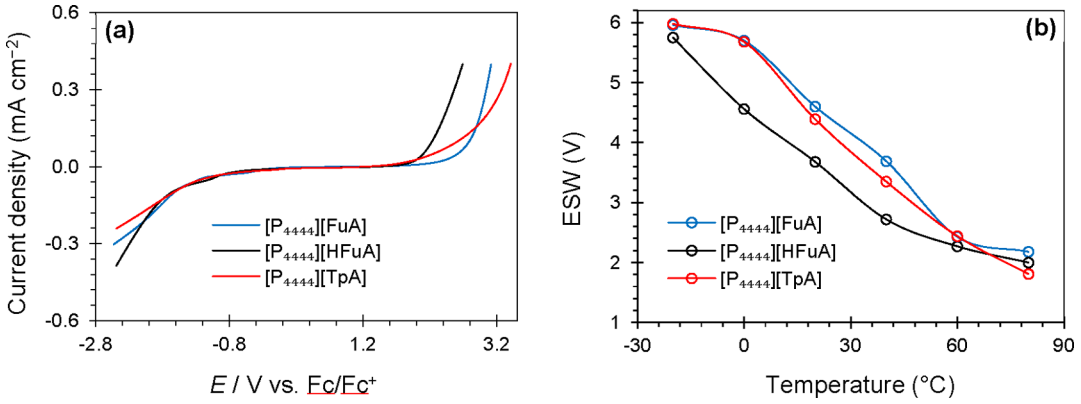

Figure 10. LSV curves at 20 mV s^{-1} and at 20 °C (a) and ESW versus temperature profiles (b) of the phosphonium-based ILs.

and [P$_{4444}$][TpA] ILs are evidently more electrochemically stable than [P$_{4444}$][HFuA] at the surface of glassy carbon electrode. The E_A is shifted to more negative by changing the anions from [FuA]$^-$ and [TpA]$^-$ to [HFuA]$^-$ and, therefore, the [P$_{4444}$][FuA] and [P$_{4444}$][TpA] ILs have wider ESW than the [P$_{4444}$][HFuA]. This is attributed to the distinct electron delocalization in [FuA]$^-$ and [TpA]$^-$ anions, which is confirmed by the ^{13}C NMR data in Figure 2, stretching shifts of C═O in the FTIR spectra in Figure 3 and the molecular electrostatic potential contours of these three anions shown in Figure 4 and Figure 5.

The temperature-dependent LSV profiles of these ILs in the temperature from −20 to 80 °C are shown in Figure S19 and the ESW values are given in Table S4. The ESWs of [P$_{4444}$][FuA] and [P$_{4444}$][TpA] are much wider than [P$_{4444}$][HFuA] in the whole studied temperature range. For instance, the ESWs of [P$_{4444}$][FuA], [P$_{4444}$][TpA], and [P$_{4444}$][HFuA] are 4.60, 4.60, and 3.95 V, respectively, at 20 °C. The ESW for each IL is getting narrower with increasing temperatures; i.e., the [P$_{4444}$][FuA] has ESW of 4.60 V at 20 °C, 3.69 at 40 °C, 2.43 V at 60 °C, and 2.18 V at 80 °C. A continuous decrease in the ESWs with an increase in temperature is previously observed for ether and siloxane functionalized imidazolium TFSI ILs.[62] Figure 10b shows the decrease in ESW as a function of temperature, with a large decrease observed between 10 and 70 °C. The decrease in ESW with temperature can be associated with the decrease in viscosity resulting in a higher ionic conductivity and diffusivity of ions and thus frequent interactions of ions with the electrode surface. Both the E_A and E_C are affected with temperature, showing that both anions and cations are sensitive to the temperature increase.[63] Traces of water can also decrease the ESW of ILs.[64] It is well-known that water molecules present heterogeneous structures and dynamics in the cavities of IL matrices and are strongly bounded to neighboring ionic groups via preferential hydrogen bonding interactions.[65] In most cases, such interactions are so strong that it is impossible to completely remove traces of these dispersed water molecules even by using high temperature and vacuum. Hence, a shoulder around 1.7 V versus Fc/Fc$^+$ in the LSV curves of both [P$_{4444}$][FuA] and [P$_{4444}$][TpA] (Figure S19a,c) that is more obvious at 60 and 80 °C might be due to the trapped water molecules' electrolysis at the electrode surface.[66] The LSV thermo-electrochemical stabilities are in very good agreement with the TGA thermal stabilities of the synthesized ILs. On the basis of these physicochemical and electrochemical investigations, it is worth mentioning that the halogen-free phosphonium-based ILs of this study can be promising electrolytes for high-temperature electrochemical devices in particular to supercapacitors and batteries.

CONCLUSIONS

A combined experimental and theoretical study has found that the nature of cation and anion, and an electron delocalization in the anion, has significant effect on the physical and electrochemical properties of ILs. The thermal analysis revealed that the tetra(*n*-butyl)phosphonium-based ILs are thermally more stable and have lower glass transition temperatures than the tetra(*n*-butyl)ammonium-based ILs having common anions. The aromatic structure of 2-furoate and thiophene-2-carboxylate anions enhanced the electrostatic interaction with cations that resulted in highly stable ILs. The aromatic anions ([FuA]$^-$ and [TpA]$^-$) based ILs are more thermally stable and presented a wider electrochemical window than nonaromatic anion ([HFuA]$^-$) based IL. This is probably due to the aromatic stability of the 2-furaote and thiophene-2-carboxylate anions that enhanced the overall stability of the ILs. As expected, the mobility of anion containing sulfur atom, [TpA]$^-$, is found to be slower than the anion with an oxygen atom, [FuA]$^-$. The anion structures have shown a pronounced effect on the oxidative limit of these ILs. In addition, [FuA]$^-$ and [TpA]$^-$ anions-based ILs have relatively wider electrochemical windows than the IL with [HFuA]$^-$ due to their distinct aromatic structural effect. The new anions presented in this study will help researchers to develop new ionic liquids with promising physicochemical and electrochemical properties that can be utilized as electrolytes for energy applications.

ASSOCIATED CONTENT

Supporting Information

The Supporting Information is available free of charge at https://pubs.acs.org/doi/10.1021/acs.jpcb.0c08421.

^{1}H, ^{13}C, ^{31}P NMR, MS-EIS, and FTIR spectra and data, details of synthesis procedures, and physicochemical and electrochemical characterizations of the ILs (PDF)

AUTHOR INFORMATION

Corresponding Authors

Faiz Ullah Shah − *Chemistry of Interfaces, Luleå University of Technology, SE-97187 Luleå, Sweden;* orcid.org/0000-0003-3652-7798; Phone: +46920491291; Email: faiz.ullah@ltu.se

https://dx.doi.org/10.1021/acs.jpcb.0c08421
J. Phys. Chem. B 2020, 124, 11962−11973

Inayat Ali Khan − *Chemistry of Interfaces, Luleå University of Technology, SE-97187 Luleå, Sweden;* orcid.org/0000-0002-7940-7297; Phone: +46920491738; Email: inayat.khan@ltu.se

Authors

Oleg I. Gnezdilov − *Institute of Physics, Kazan Federal University, 420008 Kazan, Russia*

Yong-Lei Wang − *Department of Materials and Environmental Chemistry, Arrhenius Laboratory, Stockholm University, SE-106 91 Stockholm, Sweden;* orcid.org/0000-0003-3393-7257

Andrei Filippov − *Chemistry of Interfaces, Luleå University of Technology, SE-97187 Luleå, Sweden; Medical and Biological Physics, Kazan Medical University, 420012 Kazan, Russia;* orcid.org/0000-0002-6810-1882

Complete contact information is available at: https://pubs.acs.org/10.1021/acs.jpcb.0c08421

Notes

The authors declare no competing financial interest.

■ ACKNOWLEDGMENTS

The Kempe Foundation in memory of J. C. and Seth M. Kempe is gratefully acknowledged for the financial support in the form of a stipend for I.A.K. (Grant No. SMK-1838). The financial support from the Swedish Research Council (Project No. 2018-04133) is gratefully acknowledged for supporting this work. Y.-L.W. gratefully acknowledges financial support from Knut and Alice Wallenberg Foundation (Grant No. KAW 2018.0380). O.I.G. acknowledges the subsidy allocated to the Kazan Federal University for the state assignment in the sphere of scientific activities (project number: 0671-2020-0051).

■ REFERENCES

(1) Zhang, J.; Bond, A. M. Practical Considerations Associated With Voltammetric Studies in Room Temperature Ionic Liquids. *Analyst* **2005**, *130*, 1132−1147.

(2) Quinn, B. M.; Ding, Z.; Moulton, R.; Bard, A. J. Novel Electrochemical Studies of Ionic Liquids. *Langmuir* **2002**, *18*, 1734−1742.

(3) Fuller, J.; Carlin, R. T.; Osteryoung, R. A. The Room Temperature Ionic Liquid 1-Ethyl-3-Methylimidazolium Tetrafluoroborate: Electrochemical Couples and Physical Properties. *J. Electrochem. Soc.* **1997**, *144*, 3881−3885.

(4) Wang, Y.-L.; Li, B.; Sarman, S.; Mocci, F.; Lu, Z.-Y.; Yuan, J.; Laaksonen, A.; Fayer, M. D. Microstructural and Dynamical Heterogeneities in Ionic Liquids. *Chem. Rev.* **2020**, *120*, 5798−5877.

(5) Ue, M.; Takeda, M.; Toriumi, A.; Kominato, A.; Hagiwara, R.; Ito, Y. Application of Low-Viscosity Ionic Liquid to the Electrolyte of Double-Layer Capacitors. *J. Electrochem. Soc.* **2003**, *150*, A499−A502.

(6) Sato, T.; Masuda, G.; Takagi, K. Electrochemical Properties of Novel Ionic Liquids for Electric Double-Layer Capacitor Applications. *Electrochim. Acta* **2004**, *49*, 3603−3611.

(7) Sakaebe, H.; Matsumoto, H.; Tatsumi, K. Discharge-Charge Properties of Li/$LiCoO_2$ Cell Using Room Temperature Ionic Liquids (RTILs) Based On Quaternary Ammonium Cation: Effect of the Structure. *J. Power Sources* **2005**, *146*, 693−697.

(8) Matsumoto, H.; Sakaebe, H.; Tatsumi, K.; Kikuta, M.; Ishiko, E.; Kono, M. Fast Cycling of Li/$LiCoO_2$ Cell with Low-Viscosity Ionic Liquids Based On Bis(fluorosulfonyl)imide $[FSI]^-$. *J. Power Sources* **2006**, *160*, 1308−1313.

(9) Kawano, R.; Matsui, H.; Matsuyama, C.; Sato, A.; Susan, M. A. B. H.; Tanabe, N.; Watanabe, M. High Performance Dye-Sensitized Solar Cells Using Ionic Liquids As Their Electrolytes. *J. Photochem. Photobiol., A* **2004**, *164*, 87−92.

(10) Mikoshiba, S.; Murai, S.; Sumino, H.; Kado, T.; Kosugi, D.; Hayase, S. Ionic Liquid Type Dye-Sensitized Solar Cells: Increases in Photovoltaic Performances by Adding a Small Amount of Water. *Curr. Appl. Phys.* **2005**, *5*, 152−158.

(11) Tsunashima, K.; Sugiya, M. Physical and Electrochemical Properties of Low-Viscosity Phosphonium Ionic Liquids as Potential Electrolytes. *Electrochem. Commun.* **2007**, *9*, 2353−2358.

(12) Tsunashima, K.; Sugiya, M. Physical and Electrochemical Properties of Room Temperature Ionic Liquids Based on Quaternary Phosphonium Cations. *Electrochemistry* **2007**, *75*, 734−726.

(13) Fraser, K. J.; MacFarlane, D. R. Phosphonium-Based Ionic Liquids: An Overview. *Aust. J. Chem.* **2009**, *62*, 309−321.

(14) Bradaric, C. J.; Downard, A.; Kennedy, C.; Robertson, A. J.; Zhou, Y. Industrial Preparation of Phosphonium Ionic Liquids. *Green Chem.* **2003**, *5*, 143−152.

(15) Del Sesto, R. E.; Corley, C.; Robertson, A.; Wilkes, J. S. Tetraalkylphosphonium-Based Ionic Liquids. *J. Organomet. Chem.* **2005**, *690*, 2536−2542.

(16) Fraser, K. J.; Izgorodina, E. I.; Forsyth, M.; Scott, J. L.; MacFarlane, D. R. Liquids Intermediate Between "Molecules" and "Ionic" Liquids: Liquid Ion Pairs. *Chem. Commun.* **2007**, 3817−3819.

(17) Tsunashima, K.; Niwa, E.; Kodama, S.; Sugiya, M.; Ono, Y. Thermal and Transport Properties of Ionic Liquids Based on Benzyl-Substituted Phosphonium Cations. *J. Phys. Chem. B* **2009**, *113*, 15870−15874.

(18) Duffy, N. W.; Bond, A. M. Macroelectrode Voltammetry in Toluene Using a Phosphonium-Phosphate Ionic Liquid as the Supporting Electrolyte. *Electrochem. Commun.* **2006**, *8*, 892−898.

(19) Pringle, J. M.; MacFarlane, D. R.; Forsyth, M. Solid State NMR Analysis of Polypyrrole Grown in a Phosphonium Ionic Liquid. *Synth. Met.* **2005**, *155*, 684−689.

(20) Frackowiak, E.; Lota, G.; Pernak, J. Room Temperature Phosphonium Ionic Liquids for Supercapacitor Application. *Appl. Phys. Lett.* **2005**, *86*, 164104.

(21) Khan, I. A.; Shah, F. U. Fluorine Free Ionic Liquid-Based Electrolyte for Supercapacitors Operating at Elevated Temperatures. *ACS Sustainable Chem. Eng.* **2020**, *8*, 10212−10221.

(22) Ramirez, R. E.; Sanchez, E. M. Molten Phosphonium Iodides as Electrolytes in Dye-Sensitized Nanocrystalline Solar Cells. *Sol. Energy Mater. Sol. Cells* **2006**, *90*, 2384−2390.

(23) Ramirez, R. E.; Torres-Gonzalez, L. C.; Sanchez, E. M. Electrochemical Aspects of Asymmetric Phosphonium Ionic Liquids. *J. Electrochem. Soc.* **2007**, *154*, B229−B233.

(24) Keglevich, G.; Baan, Z.; Hermecz, I.; Novak, T.; Odinets, I. L. The Phosphorous Aspect of Green Chemistry: The Use of Quaternary Phosphonium Salts and 1,3-Dialkylimidazolium Hexafluorophosphates in Organic Synthesis. *Curr. Org. Chem.* **2007**, *11*, 107−126.

(25) Matsumoto, H.; Sakaebe, H.; Tatsumi, K. Preparation of Room Temperature Ionic Liquids Based On Aliphatic Onium Cations and Asymmetric Amide Anions and Their Electrochemical Properties as a Lithium Electrolyte. *J. Power Sources* **2005**, *146*, 45−50.

(26) Kagimoto, J.; Fukumoto, K.; Ohno, H. Effect of Tetrabutylphosphonium Cation on the Physicochemical Properties of Amino-Acid Ionic Liquids. *Chem. Commun.* **2006**, 2254−2256.

(27) Shah, F. U.; Gnezdilov, O. I.; Filippov, A. Ion Dynamics in Halogen-Free Phosphonium Bis(Salicylato)Borate Ionic Liquid Electrolytes for Lithium-Ion Batteries. *Phys. Chem. Chem. Phys.* **2017**, *19*, 16721−16730.

(28) Sun, L.; Morales-Collazo, O.; Xia, H.; Brennecke, J. F. Effect of Structure on Transport Properties (Viscosity, Ionic Conductivity, and Self-Diffusion Coefficient) of Aprotic Heterocyclic Anion (Aha) Room Temperature Ionic Liquids. 2. Variation of Alkyl Chain Length in the Phosphonium Cation. *J. Phys. Chem. B* **2016**, *120*, 5767−5776.

(29) Matsumiya, M.; Suda, S.; Tsunashima, K.; Sugiya, M.; Kishioka, S.; Matsuura, H. Electrochemical Behavior of Multivalent Complexes

in Room Temperature Ionic Liquids Based On Quaternary Phosphonium Cations. *J. Electroanal. Chem.* **2008**, *622*, 129−135.
(30) Tsunashima, K.; Kawabata, A.; Matsumiya, M.; Kodama, S.; Enomoto, R.; Sugiya, M.; Kunugi, Y. Low Viscose and Highly Conductive Phosphonium Ionic Liquids Based On Bis-(fluorosulfonyl)amide Anion as Potential Electrolytes. *Electrochem. Commun.* **2011**, *13*, 178−181.
(31) Tsunashima, K.; Ono, Y.; Sugiya, M. Physical and Electrochemical Characterization of Ionic Liquids Based on Quaternary Phosphonium Cations Containing a Carbon-Carbon Double Bond. *Electrochim. Acta* **2011**, *56*, 4351−4355.
(32) Vega, J. A.; Zhou, J.; Kohl, P. A. Electrochemical Comparison and Deposition of Lithium and Potassium from Phosphonium- And Ammonium-TFSI Ionic Liquids. *J. Electrochem. Soc.* **2009**, *156*, A253−A259.
(33) Sawada, H.; Kodama, S.; Tsunashima, K.; Sugiya, M. Preparation and Properties of Novel Phosphonium-Type Ionic Liquids/Silica Gel Nanocomposite. *J. Mater. Sci.* **2007**, *42*, 2532−2535.
(34) Yamaguchi, H.; Takahashi, H.; Kato, M.; Arai, J. Lithium Tetrakis(haloacyloxy)borate: An Easily Soluble and Electrochemically Stable Electrolyte for Lithium Batteries. *J. Electrochem. Soc.* **2003**, *150*, A312−A315.
(35) Conte, L.; Gambaretto, G. P.; Caporiccio, G.; Alessandrini, F.; Passerini, S. Perfluoroalkanesulfonylimides and their Lithium Salts: Synthesis and Characterization of Intermediates and Target Compounds. *J. Fluorine Chem.* **2004**, *125*, 243−252.
(36) Omaru, A.; Nirasawa, T. Secondary Battery and Electrolyte Used Therefor. Eur. Pat. EP1318562.
(37) Barbarich, T. J.; Driscoll, P. F.; Izquierdo, S.; Zakharov, L. N.; Incarvito, C. D.; Rheingold, A. L. New Family of Lithium Salts for Highly Conductive Nonaqueous Electrolytes. *Inorg. Chem.* **2004**, *43*, 7764−7773.
(38) Armand, M.; Johansson, P. Novel Weakly Coordinating Heterocyclic Anions for Use in Lithium Batteries. *J. Power Sources* **2008**, *178*, 821−825.
(39) Jankowski, P.; Dranka, M.; Wieczorek, W.; Johansson, P. TFSI and TDI Anions: Probes for Solvate Ionic Liquid and Disproportionation-Based Lithium Battery Electrolytes. *J. Phys. Chem. Lett.* **2017**, *8*, 3678−3682.
(40) Johansson, P.; Nilsson, H.; Jacobsson, P.; Armand, M. Novel Hückel Stabilized Azole Ring-Based Lithium Salts Studied by *ab initio* Gaussian-3 Theory. *Phys. Chem. Chem. Phys.* **2004**, *6*, 895−899.
(41) Niedzicki, L.; Zukowska, G. Z.; Bukowska, M.; Szczecinski, P.; Grugeon, S.; Laruelle, S.; Armand, M.; Panero, S.; Scrosati, B.; Marcinek, M.; Wieczorek, W. New Type of Imidazole Based Salts Designed Specifically for Lithium Ion Batteries. *Electrochim. Acta* **2010**, *55*, 1450−1454.
(42) Niedzicki, L.; Kasprzyk, M.; Kuziak, K.; Żukowska, G. Z.; Armand, M.; Bukowska, M.; Marcinek, M.; Szczeciński, P.; Wieczorek, W. Modern Generation of Polymer Electrolytes Based on Lithium Conductive Imidazole Salts. *J. Power Sources* **2009**, *192*, 612−617.
(43) Niedzicki, L.; Kasprzyk, M.; Kuziak, K.; Żukowska, G. Z.; Marcinek, M.; Wieczorek, W.; Armand, M. Liquid Electrolytes Based on New Lithium Conductive Imidazole Salts. *J. Power Sources* **2011**, *196*, 1386−1391.
(44) Niedzicki, L.; Grugeon, S.; Laruelle, S.; Judeinstein, P.; Bukowska, M.; Prejzner, J.; Szczecinski, P.; Wieczorek, W.; Armand, M. New Covalent Salts of the 4+ V Class for Li Batteries. *J. Power Sources* **2011**, *196*, 8696−8700.
(45) Świderski, G.; Kalinowska, M.; Wojtulewski, S.; Lewandowski, W. The Experimental and Theoretical Study on the Influence of Alkali Metals on the Electronic Charge Distribution in Five-Membered Aromatic Acids (2-thiophenecarboxylic, 2-furanecarboxylic and 2-pyrrolecarboxylic acids). *Polyhedron* **2015**, *97*, 118−139.
(46) Lu, X.; Burrell, G.; Separovic, F.; Zhao, C. Electrochemistry of Room Temperature Protic Ionic Liquids: A Critical Assessment for Use as Electrolytes in Electrochemical Applications. *J. Phys. Chem. B* **2012**, *116*, 9160−9170.
(47) Frisch, M. J.; Trucks, G. W.; Schlegel, H. B.; Scuseria, G. E.; Robb, M. A.; Cheeseman, J. R.; Scalmani, G.; Barone, V.; Mennucci, B.; Petersson, G. A., et al. *Gaussian 16*, Revision B.1; Gaussian: Wallingford, CT, USA, 2016.
(48) Lee, C.; Yang, W.; Parr, R. G. Development of the Colle-Salvetti Correlation-Energy Formula into a Functional of the Electron Density. *Phys. Rev. B: Condens. Matter Mater. Phys.* **1988**, *37*, 785−789.
(49) Grimme, S.; Antony, J.; Ehrlich, S.; Krieg, H. A. Consistent and Accurate Ab Initio Parametrization of Density Functional Dispersion Correction (DFT-D) for the 94 Elements H-Pu. *J. Chem. Phys.* **2010**, *132*, 154104.
(50) Wang, Y.-L.; Shah, F. U.; Glavatskih, S.; Antzutkin, O. N.; Laaksonen, A. Atomistic Insight into Orthoborate-Based Ionic Liquids: Force Field Development and Evaluation. *J. Phys. Chem. B* **2014**, *118*, 8711−8723.
(51) Abraham, M. J.; Murtola, T.; Schulz, R.; Pall, S.; Smith, J. C.; Hess, B.; Lindahl, E. GROMACS: High Performance Molecular Simulations through Multi-level Parallelism from Laptops to Supercomputers. *SoftwareX* **2015**, *1*, 19−25.
(52) Daasch, L. W.; Smith, D. C. Infrared Spectra of Phosphorous Compounds. *Anal. Chem.* **1951**, *23*, 853−868.
(53) Seddon, K. R.; Stark, A.; Torres, M.-J. Influence of Chloride, Water, and Organic Solvents on the Physical Properties of Ionic Liquids. *Pure Appl. Chem.* **2000**, *72*, 2275−2287.
(54) O'Mahony, A. M.; Silvester, D. S.; Aldous, L.; Hardacre, C. R.; Compton, G. Effect of Water on The Electrochemical Window and Potential Limits of Room-Temperature Ionic Liquids. *J. Chem. Eng. Data* **2008**, *53*, 2884−2891.
(55) Xie, W.; Xie, R.; Pan, W.-P.; Hunter, D.; Koene, B.; Tan, L.-S.; Vaia, R. Thermal Stability of Quaternary Phosphonium Modified Montmorillonites. *Chem. Mater.* **2002**, *14*, 4837−4845.
(56) Fukaya, Y.; Sekikawa, K.; Murata, K.; Nakamura, N.; Ohno, H. Miscibility and Phase Behavior of Water-Dicarboxylic Acid Type Ionic Liquid Mixed Systems. *Chem. Commun.* **2007**, 3089−3091.
(57) Fukaya, Y.; Iizuka, Y.; Sekikawa, K.; Ohno, H. Bio Ionic Liquids: Room Temperature Ionic Liquids Composed Wholly Of Biomaterials. *Green Chem.* **2007**, *9*, 1155−1157.
(58) Bhattacharyya, S.; Shah, F. U. Thermal Stability of Choline Based Amino Acid Ionic Liquids. *J. Mol. Liq.* **2018**, *266*, 597−602.
(59) Deng, D.; Jiang, Y.; Liu, X. Investigation of Furoate-Based Ionic Liquid as Efficient SO_2 Absorbent. *New J. Chem.* **2017**, *41*, 2090−2097.
(60) Galinski, M.; Lewandowski, A.; Stepniak, I. Ionic Liquids as Electrolytes. *Electrochim. Acta* **2006**, *51*, 5567−5580.
(61) Shah, F. U.; Khan, I. A.; Johansson, P. Comparing the Thermal and Electrochemical Stabilities of Two Structurally Similar Ionic Liquids. *Molecules* **2020**, *25*, 2388.
(62) Chavan, S. N.; Tiwari, A.; Nagaiah, T. C.; Mandal, D. Ether and Siloxane Functionalized Ionic Liquids and their Mixtures as Electrolyte for Lithium-Ion Batteries. *Phys. Chem. Chem. Phys.* **2016**, *18*, 16116−16126.
(63) Wang, Y.-L.; Golets, M.; Li, B.; Sarman, S.; Laaksonen, A. Interfacial Structures of Trihexyltetradecylphosphonium-bis-(mandelato)borate Ionic Liquid Confined Between Gold Electrodes. *ACS Appl. Mater. Interfaces* **2017**, *9*, 4976−4987.
(64) Schröder, U.; Wadhawan, J. D.; Compton, R. G.; Marken, F.; Suarez, P. A. Z.; Consorti, C. S.; de Souza, R. F.; Dupont, J. Water-Induced Accelerated Ion Diffusion: Voltammetric Studies in 1-Methyl-3-[2,6-(S)-dimethylocten-2-Yl]-imidazolium Tetrafluoroborate, 1-Butyl-3-methyl-imidazolium Tetrafluoroborate and Hexafluorophosphate Ionic Liquids. *New J. Chem.* **2000**, *24*, 1009−1015.
(65) Wang, Y. L.; Sarman, S.; Kloo, L.; Antzutkin, O. N.; Glavatskih, S.; Laaksonen, A. Solvation Structures of Water in Trihexyltetradecylphosphonium-Orthoborate Ionic Liquids. *J. Chem. Phys.* **2016**, *145*, 064507.

https://dx.doi.org/10.1021/acs.jpcb.0c08421
J. Phys. Chem. B 2020, 124, 11962−11973

(66) Silvester, D. S.; Compton, R. G. Electrochemistry in Room Temperature Ionic Liquids: A Review and Some Possible Applications. *Z. Phys. Chem.* **2006**, *220*, 1247−1274.

https://dx.doi.org/10.1021/acs.jpcb.0c08421
J. Phys. Chem. B 2020, 124, 11962−11973